PERGAMON

Journal of Structural Geology 25 (2003) 1841–1854

JOURNAL OF STRUCTURAL GEOLOGY

www.elsevier.com/locate/jsg

Strain paths of three small folds from the Appalachian Valley and Ridge, Maryland

Carol J. Ormand[a,*], Peter J. Hudleston[b]

[a]*Department of Geology, Wittenberg University, Springfield, OH 45501-0720, USA*
[b]*Department of Geology and Geophysics, University of Minnesota, Minneapolis, MN 55455, USA*

Received 7 February 2002; received in revised form 10 May 2002; accepted 10 February 2003

Abstract

Structural analysis indicates that, for a given set of conditions, subtle differences in layer configuration and rheology can result in major differences in fold kinematics. We studied three hand-sample scale folds from the Maryland Valley and Ridge province in an effort to understand the accommodation of folding on meso- and microscopic scales, and to constrain the deformation histories of the folds sampled. Two single-layer folds and one multilayer fold were taken from two nearby outcrops of the Wills Mountain Anticline, and are therefore interpreted to have developed under virtually identical pressure and temperature conditions. Although all three folds are dominated by carbonate material, structural fabrics are unique for each fold, indicating rheological contributions to and local structural control of fabric development. Both single layer folds have asymmetric vein distributions that are consistent with strain directions expected from asymmetric flexural flow. Slickenlines (on one sample) and cleavage in an adjacent layer (in the other sample) support this interpretation. The first of these folds appears to have undergone late-stage hinge tightening, as evidenced by the development of crosscutting bed-normal stylolites. In contrast, veins, stylolites, and the intracrystalline deformation in the multilayer fold are suggestive of (symmetric) tangential longitudinal strain followed by heterogeneous sub-horizontal flattening. The three folds are interpreted to be buckle folds, with differing mechanisms accommodating strain within the competent layers.

Keywords: Strain paths; Structural fabrics; Rheology

1. Introduction

Comparable finite fold geometries may develop through various deformation histories. However, structural fabrics within folded rocks can be used to infer the incremental and cumulative strain, and thus the strain history (cf. Groshong Jr., 1975; Onasch, 1984; Dietrich, 1986; Narahara and Wiltschko, 1986). One can then evaluate the application of various kinematic models to the fold in question (e.g. Simon and Gray, 1982; Markley and Wojtal, 1996; McConnell et al., 1997; Thorbjornsen and Dunne, 1997). We compared fabric distributions in three small-scale folds from the Appalachian Valley and Ridge Province with strain distributions predicted for several different kinematic models of folding. Because the dominant structures in our sample folds are veins and stylolites, we include predicted orientations of these structures for each of the kinematic models.

Common kinematic models for fold development, described in detail below, include tangential longitudinal strain (also called orthogonal flexure) (Fig. 1a; e.g. Ramsay, 1967, pp. 397–403), inner-arc collapse (Fig. 1b; Hudleston and Lan, 1993), flexural flow and flexural slip (Fig. 1c; e.g. Ramsay, 1967, pp. 391–393). All of these involve overall shortening of the strata, in response to bending or buckling stresses. Each model has predictable distributions of finite strain, and thereby of possible accommodation structures. We neglect passive-shear folding, as it occurs in layers where competence contrast is negligible, and the sample folds we selected are from units more competent than the layers encasing them.

Tangential longitudinal strain (Fig. 1a) involves extension of the outer arc and shortening of the inner arc of a fold, with the zones of extension and shortening separated by a neutral surface, where finite strain is zero. If there is no overall transport of material from inner arc to outer arc, the finite neutral surface migrates toward the outer arc (with respect to an external frame of reference), and the outer arc

* Corresponding author.
E-mail address: cormand@wittenberg.edu (C.J. Ormand).

0191-8141/03/$ - see front matter © 2003 Elsevier Ltd. All rights reserved.
doi:10.1016/S0191-8141(03)00042-7

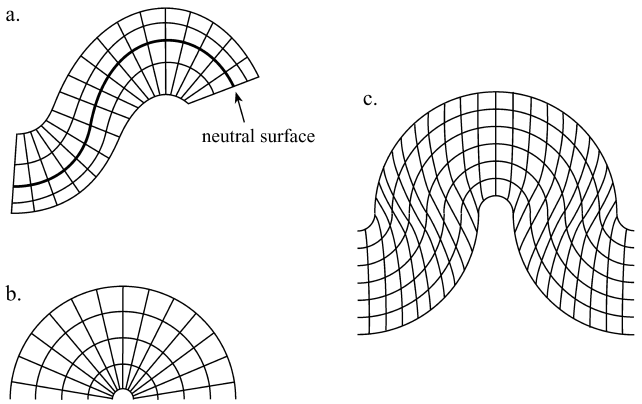

Fig. 1. Models of strain in folded rocks. Grid lines in each model represent originally orthogonal material lines. (a) Tangential longitudinal strain. The neutral surface is the material line of no finite elongation; it may or may not migrate away from the center of the layer during deformation. (b) Inner arc collapse. (c) Flexural flow. ((a) and (c) Modified from Ramsay (1967); (b) after Hudleston and Lan (1993).)

thins while the inner arc thickens (Ramsay, 1967). If the shortening is accomplished by dissolution of inner arc material, which is transported and precipitated in the outer arc, the neutral surface may remain in a central location (Hudleston and Tabor, 1988). In either case, principal strain directions remain parallel and perpendicular to layering throughout deformation (Fig. 1a). Thus, stylolites and veins would develop normal to bedding in the inner and outer arcs, respectively.

When tangential longitudinal strain is accompanied by volume change, related structures may predominate. For example, in the case of overall volume gain, deformation may be accommodated through vein development in the outer arc, with thrusting in the inner arc. Or, with overall volume loss, stylolites may develop normal to layering throughout the layer, with the outer arc acting as the neutral surface; this is called inner-arc collapse (Fig. 1b; Hudleston and Tabor, 1988). Whether tangential longitudinal strain involves volume change or not, principal strain axes remain parallel and perpendicular to layering throughout deformation, so the resulting accommodation structures have predictable positions and orientations relative to the fold.

Flexural flow or flexural slip processes may accomplish similar overall changes in shape. Flexural flow (Fig. 1c) involves the homogeneous flow of material, parallel to layering and either normal or oblique to fold hinges. It results in ductile deformation accommodating predictable amounts of simple shearing (Ramsay, 1967, pp. 391–393). This results in principal strain axes that are oblique to bedding planes (Fig. 1c). The shearing may be accommodated by such structures as en échelon veins in each limb of the fold, dipping toward the axial surface. In flexural slip folds, the same flexure of layers develops by layer-parallel slip occurring between the layers (Ramsay, 1967, p. 392). Associated structures include slickenlines on bedding surfaces. Of course, if a multilayer fold deforms by flexural slip, the individual layers within it will also deform internally.

Flexural flow may be symmetrical or asymmetrical (e.g. Ramsay, 1967, p. 391; Geiser et al., 1988; Fisher and Anastasio, 1994). In symmetrical flexural flow, folded layers are locally pinned at the axial plane, and shear directions are in opposite directions on either side of the axial surface. In asymmetric flexural flow, the layers are locally pinned on one limb of the fold, concentrating deformation in the other limb. Given a local pin location, shear strain distribution in a flexural fold depends on fold geometry, and one can infer the orientations of structures that might accommodate shape changes in the deforming layers.

In this study, we illustrate the use of fabric distributions in distinguishing the deformation histories of a few natural folds. Identical finite fold geometries may develop through a variety of different processes. However, each process would result in a predictable and recognizable suite of structures. We apply this idea to three small-scale folds in sedimentary strata of the Valley and Ridge province of the Appalachians. We analyze geometry and fabric in both single layer and multilayer folds, for three different fold shapes. Using fabrics, we gain information on the incremental and cumulative strain, and thus the strain history (cf. Groshong Jr., 1975; Onasch, 1984; Dietrich, 1986; Narahara and Wiltschko, 1986). Fabric distributions in our single-layer folds best fit a model of asymmetric flexural flow, while fabrics in the multilayer fold suggest a history of tangential longitudinal strain followed by flattening. This type of analysis provides a reliable basis for the interpretation of natural folds and fabrics, and thus of the mechanical response of layered rocks to deformation.

2. Geological setting

The small-scale folds described in this study were taken from the flanks of the Wills Mountain Anticline. This anticline is on the western edge of the Appalachian Valley and Ridge province (Fig. 2), which extends eastward to the North Mountain thrust (Figs. 2 and 3). In the region of this study, the axis of the Wills Mountain Anticline is discontinuous (Scott and Dunne, 1990; Fig. 3a). The anticline is part of the surface expression of a fault-bend fold in the lower Paleozoic section (Dunne, 1989; Fig. 3b). This underlying fold-fault system verges northwestward, in the regional transport direction. Hence, the southeastern limb of the anticline dips more gently than the northwestern limb.

The underlying fault-bend fold is part of a blind duplex (Perry, 1978; Kulander and Dean, 1986; Mitra, 1986; Ferrill and Dunne, 1989). The floor detachment is in the Cambrian Waynesboro shales, whereas the middle Ordovician Martinsburg Formation contains the roof thrust. Cambro-Ordovician carbonates form the horses

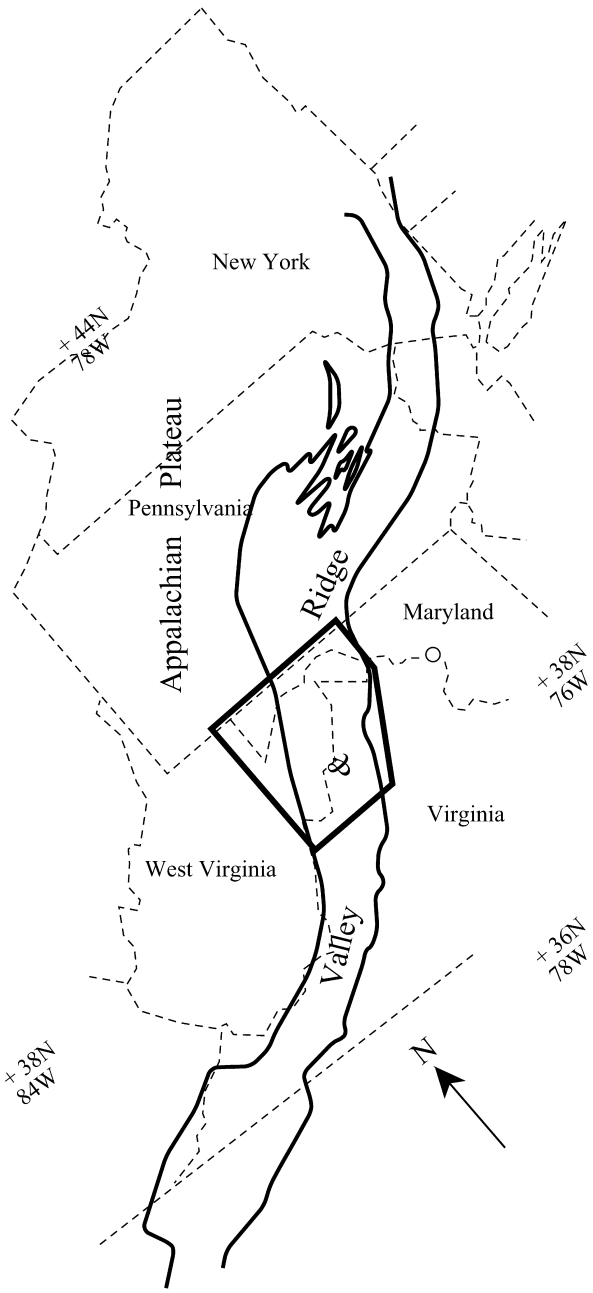

Fig. 2. Provinces of the Appalachian orogen. Box shows the area of the map in Fig. 3. (Modified from Engelder (1989).)

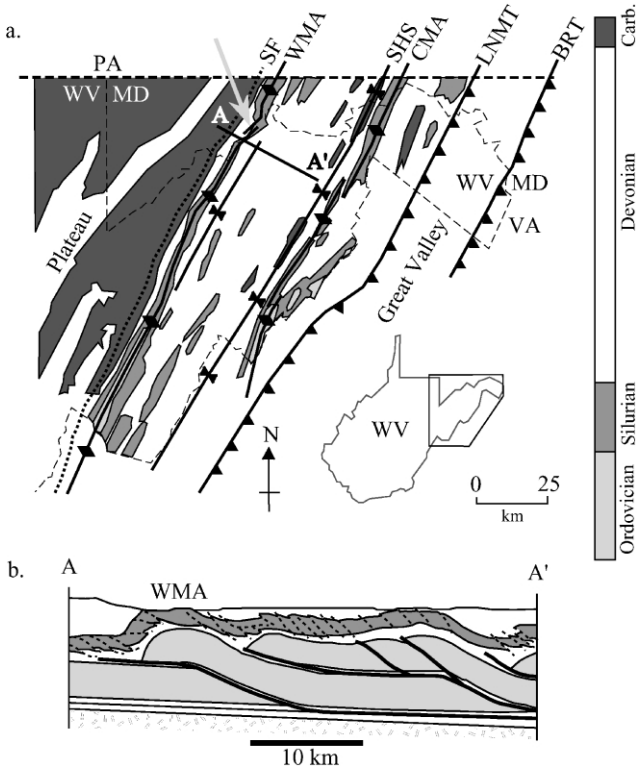

Fig. 3. (a) Geological map and stratigraphy for eastern West Virginia and surrounding areas. Arrow points to the study area. A–A′ is the line of cross-section shown in (b). SF = Alleghanian Structural Front; WMA = Wills Mountain Anticline; SHS = Sideling Hill Syncline; CMA = Cacapon Mountain Anticline; LNMT = Little North Mountain Thrust; BRT = Blue Ridge Thrust. (From Dunne (1989).) (b) Cross-section through the West Virginia Valley and Ridge. Light gray = Cambro-Ordovician carbonates, dark gray = upper Ordovician-lower Devonian component of roof sequence (from Wilson and Shumaker (1992)).

of the duplex system, accommodating a total shortening of about 40% (Dunne, 1989, 1996; Wilson and Shumaker, 1992). The cover rocks are decoupled from the underlying duplex system along the roof thrust in the Martinsburg Formation, allowing shortening in the cover to be accommodated differently than in the Cambro-Ordovician carbonates (Banks and Warburton, 1986; Dunne and Ferrill, 1988; Geiser, 1988a,b; Ferrill and Dunne, 1989; Groshong Jr. and Epard, 1992; Dunne, 1996; Smart et al., 1997).

Temperature and pressure of deformation for the cover rocks are not well constrained. Coexisting aqueous (brine) fluid and methane inclusions in vein minerals in the Silurian Clinton Formation through the Lower Devonian Helderberg Formation of the Wills Mountain Anticline record trapping temperatures of 85–155 °C and pressures of 50–150 MPa (Evans, 1998, personal communication). While these are wide ranges, we suggest that the similarity of structural positions of our samples makes it likely that they all deformed under similar temperature and pressure conditions.

3. The folds

Three hand-sample-scale folds were collected from the flanks of the Wills Mountain Anticline. Fold A is from Cedar Cliff, on the eastern limb of the Wills Mountain Anticline, whereas B and C are from Pinto, on the western limb of the anticline (Fig. 4). Folds A and C (Fig. 5a and c) are from the Silurian McKenzie Formation, and B (Fig. 5b) is from the Silurian Wills Creek Formation. Both formations consist of interbedded limestones and mudstones.

Fold A is a single-layer fold (Fig. 5a). Hinge shape, overall, is mildly box-like, with the fold verging to the west.

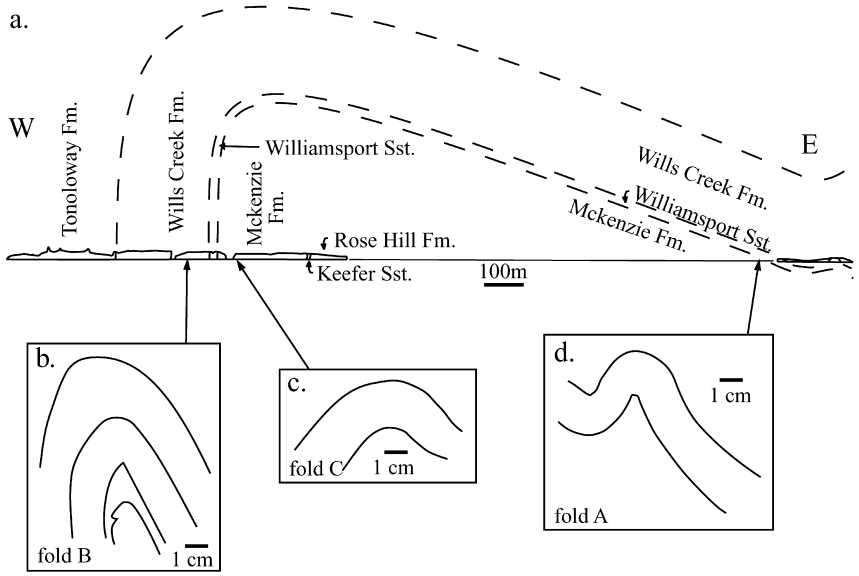

Fig. 4. (a) Schematic cross-section, projecting outcrops at Pinto (western limb) and Cedar Cliff (eastern limb) onto a vertical plane normal to strike. Actual fold structure is more complicated than depicted here. (b)–(d) Line sketches of sample locations and orientations.

A striking fabric asymmetry reflects the asymmetry of the fold shape. Veins are concentrated in the short limb of the fold, but are not oriented consistently with respect to bedding. Rather, they are subnormal to the fold axial plane. Some shear zones/faults are developed within the veins, as are a small number of twins. Slickenlines perpendicular to the fold hinges occur on one of the inner-arc bedding surfaces. Stylolites are primarily normal to bedding and define packets of different bedding orientation within the fold. However, bedding curves gently in each packet, so bedding dip is not constant between stylolites (Fig. 6). Two major stylolites occur where 'box' fold hinges would be (Fig. 5a).

Fold B is multilayered (Fig. 5b). Veins are quite common, generally perpendicular to layering, and are wider in the outer arc and narrower in the inner arc of each layer, especially where curvature is pronounced. Vein density is slightly higher in the hinge region than in the limbs. Stylolites are mostly parallel to bedding. Undulose extinction of vein calcite is ubiquitous, whereas twins are rare.

Fold C is another single-layer fold (Fig. 5c). It is fairly smooth, with a rounded hinge zone and, for the segment available, an apparently symmetric shape. However, only one limb has a series of en échelon veins and fractures, dipping toward the axial surface. Also, an inner layer shows cleavage approximately normal to the veins, and inclined relative to the fold axial plane.

The two single-layer folds (A and C) show asymmetric distributions of meso- and microstructures, whereas the multilayer fold (B) has both a symmetric shape and greater structural symmetry. All three have rounded to subrounded hinges, with intralayer deformation accommodated largely by veining and pressure solution.

4. Methods and models

For each of our three fold samples, we compared the distribution of structures with the strain distributions associated with possible kinematic models. We scanned thin sections of each fold to obtain images of fold shape, primary layering, veins, and stylolite seams (Fig. 5). We then attempted to find best-fit circular arcs for the fold shapes, using the same center of curvature points for as much of each fold as possible (Fig. 7). We used these idealized fold shapes to model strain distributions around each fold, based on predictions of fold development in various models. Comparing the observed structures with strain distributions for the kinematic models, we can eliminate unlikely fold kinematics where the structures do not match predicted strains (Oertel, 1974; Yin and Oertel, 1993). We focused on matching vein and stylolite distributions and orientations to the strain predictions because these are the primary observed structures of intralayer deformation in the folds studied. We have not attempted to include deformation accommodated by such structures as interlayer slickenlines (fold A) and undulose extinction (fold B). Thus, we expect a qualitative, rather than quantitative, match between our observed and predicted suites of veins and stylolites attributable to a particular folding model.

4.1. Tangential longitudinal strain

One model we applied to each fold was that of tangential

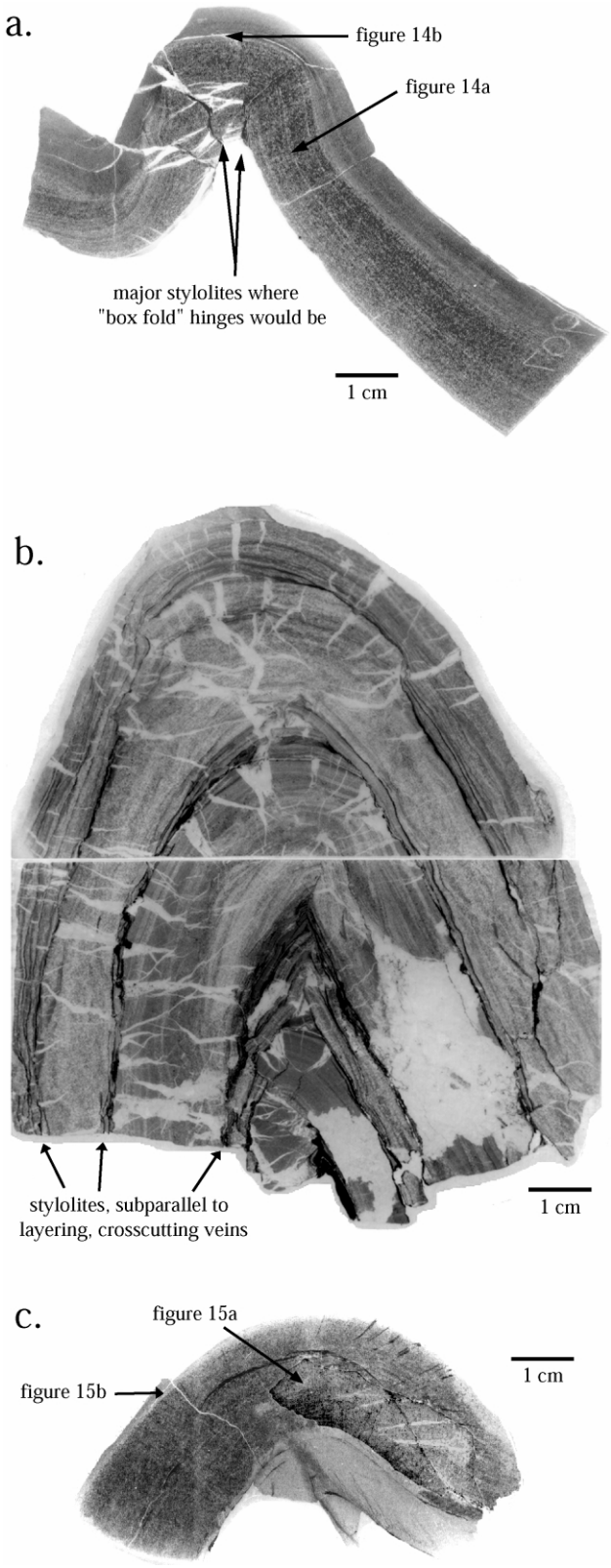

Fig. 5. Scanned images of the three folds, looking north at each. (a) Fold A; arrows indicate locations of microprobe images in Fig. 14. (b) Fold B. (c) Fold C; arrows indicate locations of microprobe images in Fig. 15. A zone of chemical alteration has been darkened for clarity. Each scale bar is 1 cm long.

longitudinal strain (Ramsay, 1967, pp. 397–398; Fig. 1a). Tangential longitudinal strain involves extending the outer arc and commensurably shortening the inner arc of a folded layer. To keep the model simple, we assumed the neutral surface maintained a central position during deformation (Hudleston and Tabor, 1988). To ascertain what strain distribution could be expected for the curvature of each sample fold, we arbitrarily divided each fold into four equi-thickness reference layers, then drew line segments normal to the central curve that intersected it at regular intervals. That is, we established a 'deformed grid' that would correspond to a perfectly square grid if the fold was 'unfolded' to an undeformed state, assuming the unfolding occurred by removing tangential longitudinal strain. We then fitted strain ellipses to each box of the grid (e.g. Fig. 8a). Finally, assuming this strain distribution was accommodated entirely by veins and stylolites, we superimposed veins in the outer arc and stylolites in the inner arc of the gridded fold (e.g. Fig. 8a).

Whereas the thickness and density of stylolites is controlled by compositional impurity of the folded layer, vein thickness is directly computable, by measuring the extension of the outer arc and assuming a number of veins. Our choice of vein density is somewhat arbitrary but the proportion of vein material to host rock is constrained (assuming no internal deformation of the vein material). Just as veins are thicker toward the outer arc and thinnest at the neutral surface, stylolites should increase in thickness or amplitude away from the neutral surface, in a homogeneous material, reflecting the relative volume of host rock lost to pressure solution. And, of course, both stylolites and veins are normal to bedding in this model.

4.2. Flexural flow and flexural slip

The next models we applied to each fold were flexural flow and flexural slip. Flexural slip involves the sliding of layers past each other as each layer bends, analogous to the sliding of cards in a deck as they are made to bend. Flexural flow is a homogeneously distributed shearing that accomplishes the same change in shape as flexural slip, but without localized slip surfaces. One key aspect of this folding mechanism is that there is a pin line (assumed here to be normal to bedding), where shear strain is non-existent and away from which shear strain increases. Fold B lacked undeformed regions, so we did not analyze it using this kinematic model (Fig. 5b).

For the other two folds, we again began by establishing a grid of 'deformed squares' on the fold shape, measured from the pin line (Geiser et al., 1988). Classical flexural flow or slip assumes the pin line lies along the axial surface (Ramsay, 1967, p. 391; Fig. 1c). This location implies a symmetry of deformation that we do not observe in folds A and C, so we also considered pin lines elsewhere within these folds. However, the axial pin line placement illustrates a feature common to flexural flow and flexural slip:

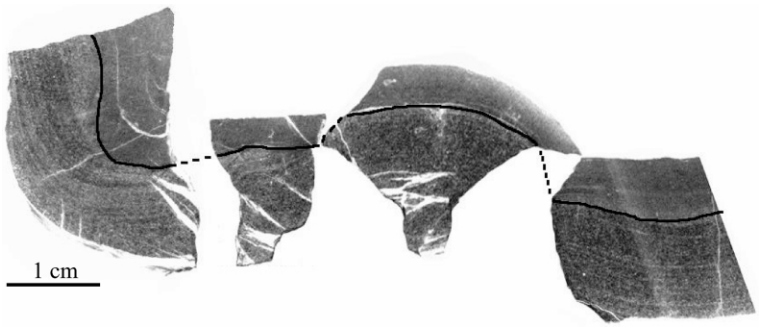

Fig. 6. Scanned image of the hinges of fold A, with curvature related to dissolution seams (stylolites) 'removed'. See text for discussion.

because principal extension directions are not layer-parallel (Fig. 1c), folding by these processes can result in en échelon veins that 'dip' toward the fold axial surface.

Asymmetric flexural flow or slip models involve a pin line on the limb of a fold (e.g. Geiser et al., 1988; Fisher and Anastasio, 1994). Ideally, we should put the pin line in the least strained region of the folded layer, but since fabric development is weak in at least one limb of folds A and C, the placement is a bit arbitrary within those relatively undeformed limbs. Fortunately, the exact location of the pin line does not strongly affect predicted strain magnitudes and orientations for these fold geometries (compare Fig. 8c and d).

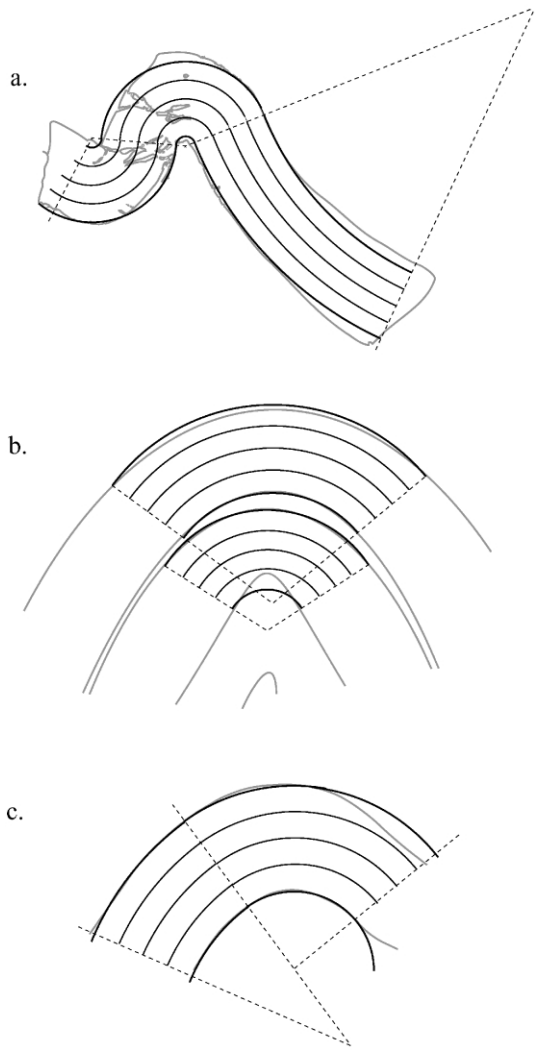

Fig. 7. Study folds with best-fit circular arcs. (a) Fold A. (b) Fold B, first 'unflattened' homogeneously. See text for discussion. (c) Fold C.

4.3. Homogeneous flattening

We also considered the possibility that these folds underwent late-stage flattening. We use the term 'flattening' to mean a coaxial deformation involving a negative stretch (change in length divided by original length) in one direction. Horizontal flattening, then, may be accomplished via volume loss, or through extension in a perpendicular direction or directions, or by a combination of volume loss and extension. A plane strain (no volume change, no out-of-plane motion) horizontal flattening might result in horizontal extensional fractures or veins, and/or stylolite seams with horizontal peaks.

4.4. Rolling hinges

Another possibility we considered is hinge migration during folding (e.g. Dewey, 1965; Suppe, 1983; Smallshire, 1997). This process is not uniquely tied to any particular fold mechanism. For example, a fold with a migrating hinge could develop by tangential longitudinal strain, flexural flow, flexural slip, or by some combination of these, and the loci of deformation could move in all cases with time (e.g. Williams, 1979; Gray, 1981; Sanderson, 1982). For example, consider a fold pair initiating in a layer via two hinges migrating away from the initiation point. If the mechanism of folding is tangential longitudinal strain, we would expect to see extensional structures not only in the outer arcs of the present hinge zones, but also in the regions through which the hinges have already migrated (Smallshire, 1997; Fig. 9a). This fold evolution could, for example, result in concentrated vein and/or stylolite development in the shorter limb of an asymmetric fold, with the majority of veins in what were previously outer-arc regions, and the majority of stylolites in what were previously inner arcs.

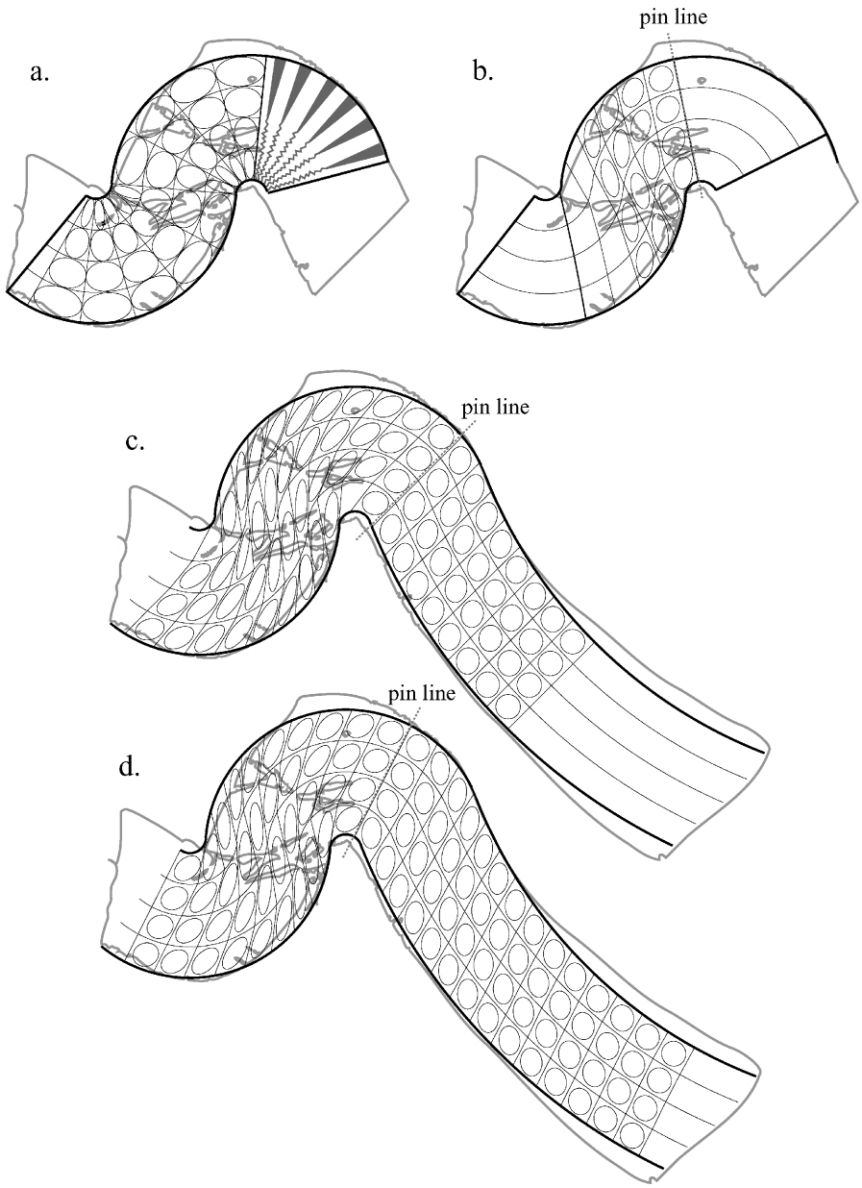

Fig. 8. Various fold models applied to fold A, with ellipses to show predicted strain magnitudes. Irregular gray lines indicate actual vein geometries. (a) Tangential longitudinal strain; wedges and jagged lines represent expected vein and stylolite geometries. (b) Flexural flow, pinned at the antiformal hinge. (c), (d) Flexural flow, pinned 'off-center'. Actual vein locations and orientations best match the asymmetric flexural flow models.

Similarly, in a fold developed by flexural flow and/or flexural slip, the hinges might migrate as the fold developed. Again, if the hinges migrated outward from a fold nucleation point, and if the shearing were accommodated by veins, en échelon vein sets would develop and migrate outward from the fold initiation point. The oldest veins, rotated to orientations at high angles to bedding, would be concentrated in the center of the shorter limb of an asymmetric fold (compare Fig. 9b–d). There are, theoretically, an infinite number of possible migrating hinge fold histories for any given fold geometry. But, given a particular history, one can infer a suite of structures that could accommodate such a history.

5. Results

5.1. Fold A

We approximated the shape of fold A with three circular arc segments (Fig. 7a). We were unable to fit thickness changes around the fold (Figs. 5a and 7a) into our simplified models, as they do not lend themselves to idealized circular arcs. Otherwise, the geometry of fold A is notable because the radii of curvature for inner and outer arcs of the anticline are the same as for the syncline.

Within fold A, the distribution of veins is limited to the short limb, rather than being equally distributed on each side of each hinge zone. As can be clearly seen, this distribution

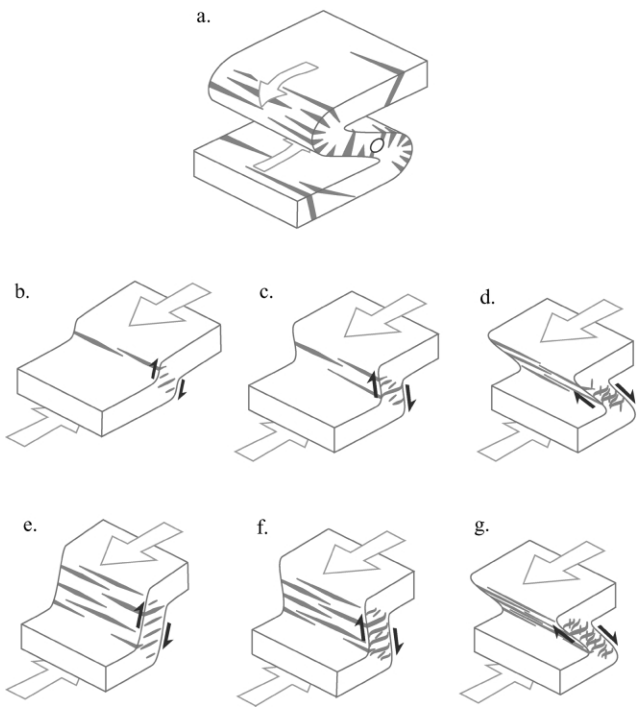

Fig. 9. A comparison of possible vein distributions in folds with rolling and fixed hinges. (a) Tangential longitudinal strain, rolling hinge. Circle represents the fold nucleation point; arrows show movement of material from fold limbs into the hinge regions. After Smallshire (1997). (b)–(d) Flexural flow, rolling hinge. Early veins are reoriented as shearing accommodates hinge migration. Highly sheared veins are concentrated near the fold nucleation point. (e)–(g) Flexural flow, fixed hinge. Highly sheared veins are evenly distributed in the short limb. Compare (d) and (g) for folds with the same shape, but different structures, especially near fold hinges.

does not match the symmetric distribution we would expect for tangential longitudinal strain (Fig. 8a). The asymmetric structural distribution is also not what we would expect for symmetric flexural flow or slip (Fig. 8b). However, the extension directions implied by vein orientations are consistent with those predicted by a flexural flow or slip model. The lack of apparent slip surfaces *within* the folded layer precludes the possibility that it deformed by flexural slip. Thus, we considered the possibility that this fold formed by flexural flow, but with the pin line(s) outside the hinge zones. As can be seen (Fig. 8c and d), the exact location of the pin line (within this moderately strained limb) does not have a large effect on strain magnitude and orientation. Both of these models of asymmetric flexural flow show a deformation concentration in the short limb, with extension directions quite consistent with observed vein orientations. Folding by flexural flow is also consistent with our observation of slickenlines parallel to bedding and perpendicular to the fold axis.

It should be noted, however, that this analysis disregards the presence of late-stage bed-perpendicular stylolites in the hinge zone of the fold. These stylolites appear to have resulted in hinge tightening, implying that curvature (and therefore strain magnitudes) due to flexure may be less than originally calculated. Similarly, observed vein widths are significantly less than we would expect from the strain ratios predicted in the asymmetric flexural flow models. However, they may be consistent with the development of a more open flexural flow fold, later tightened by localized dissolution.

5.2. Fold B

The parabolic shape of fold B does not lend itself to circular arc approximations (Fig. 5b). However, the prevalence of veins normal to bedding suggests a history involving tangential longitudinal strain, or more accurately ‘outer arc extension’, particularly since veins in the zone of highest curvature are wedge-shaped, tapering toward the inner arc of each layer (compare Figs. 5b and 10). Also, stylolites subparallel to the axial surface are common, and often crosscut other structures (Fig. 5b), which we interpret to indicate a later flattening event that modified the fold shape. So, we chose to ‘unflatten’ the fold layers in a direction normal to both the fold axial plane and the late stylolites. We used Adobe Illustrator to apply a pure shear to the fold trace until it had more or less circular arc-shaped layers (Figs. 7 and 11a). One disadvantage of this retrodeformation, discussed below, is that our ‘unflattening’ was spatially homogeneous.

Having achieved a shape that is not dissimilar from that of a parallel fold, we treated it as the pre-flattened fold shape and fit it with curves (Fig. 7b), and gridded each of the carbonate layers as with the other folds. We calculated strain ellipses and constructed representative veins and stylolites for those strains. In one model we included bed-perpendicular stylolites, although they are not common in the fold (Fig. 11b). In another model we used only veins to account for the strains (Fig. 11c), thus including volume increase in the model. We used Adobe Illustrator to re-flatten this image (Fig. 11d).

In the process of homogeneous flattening, when the host rock deforms, any passive markers oblique to the principal strain directions are reoriented (Fig. 11d). However, in fold B, veins are clearly normal to bedding. Nonetheless, stylolites and tabular veins in the limbs of the fold suggest late-stage flattening, and undulose extinction of the vein calcite is also consistent with a late- or post-folding deformation. We suggest that late-stage flattening occurred in such a way as to minimize reorientation of the veins. This could be accomplished if the flattening is somewhat less than that applied in Fig. 11, and if it is applied heterogeneously, such that the plane of flattening varies by about 25° from one limb to the other, being sub-parallel to each limb (Fig. 12). The trajectories of flattening strain would behave in this way if the core of the fold was relatively competent during deformation.

To test this idea, we next applied ‘unflattening strains’ of about 10% (axial ratio 1.2) to each flank of fold B (Fig. 12). In this model, the orientation—nearly orthogonal to

Fig. 10. Four 'layers' of fold B, with curvature accommodated by veining graphically 'removed'. Compare with Fig. 5b. Note that bed-normal veins accommodate a significant amount of curvature, but certainly not all of it.

bedding—of most of the wedge-shaped veins is the same, pre- and post-flattening. Furthermore, the thickness of the central layer (labeled in Fig. 12), the best-defined layer in the multilayer, is nearly constant in this pre-flattened state. This suggests to us a history of outer arc extension in each layer of the multilayer, followed by moderate tightening of the fold by way of 'flattening' subparallel to each fold limb. Complicating the situation is the likely localization of flattening along stylolites, which is not taken into account in Fig. 12.

5.3. Fold C

Again, we began by fitting circular arcs to the fold shape. Because the radius of curvature is not constant around the fold, we subdivided the fold into two regions with different radii of curvature. Applying the model of tangential longitudinal strain, we gridded the fold, fit theoretical strain ellipses, calculated extension of the outer arc, and inferred vein thickness (dependent on the number of veins) (Fig. 13a). This predicted structural geometry does

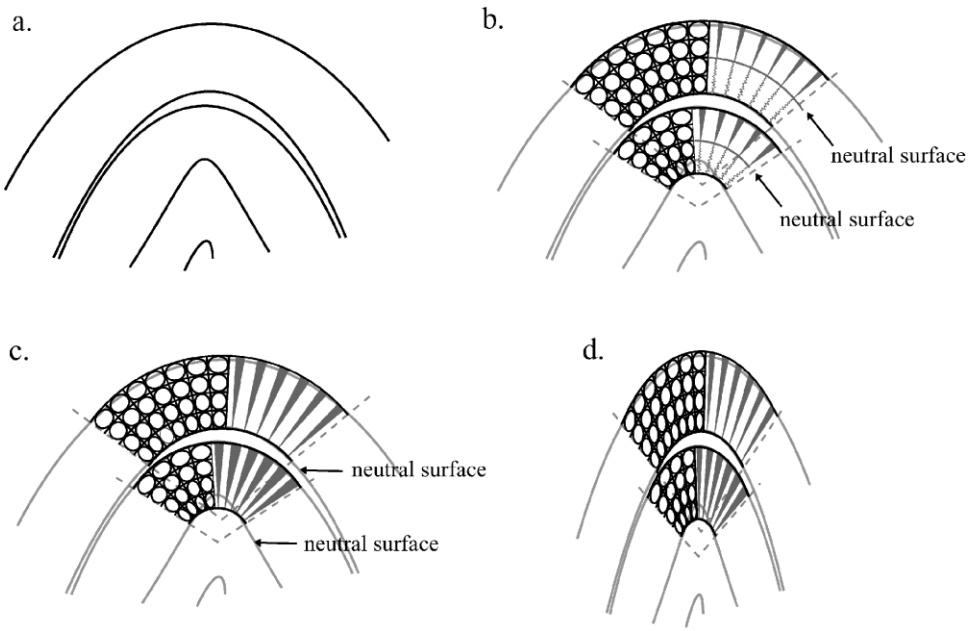

Fig. 11. Various fold models applied to fold B. (a) Homogeneously 'unflattened'. See text for discussion. (b) Tangential longitudinal strain prior to flattening. (c) Outer-arc stretching prior to flattening. (d) Outer-arc stretching followed by homogeneous flattening.

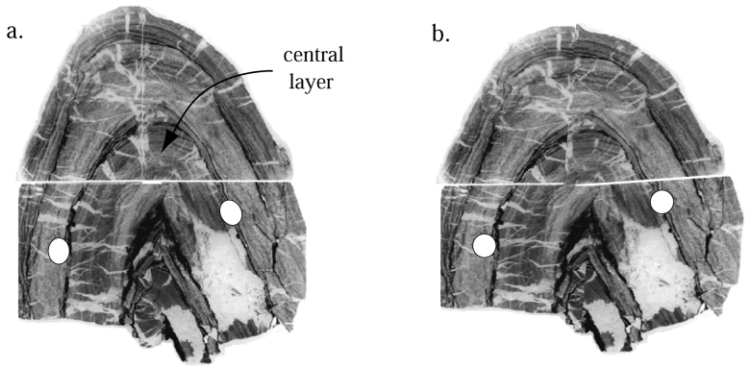

Fig. 12. Heterogeneous unflattening of fold B. (a) Fold B; stylolites suggest that most of the late-stage flattening occurred normal to bedding, as mimicked by the strain ellipses shown here. Those planes of flattening differ in orientation by approximately 24°. (b) 'Unflattening' each flank of the fold independently does not reorient veins. See text for discussion.

not particularly fit the distribution and orientation of structures. We next tried a flexural flow model (Fig. 12b). The en échelon veins of the fold would seem to fit asymmetric flexural flow models quite nicely, with veins present on only one side of the fold. Trying various 'one-sided' pin lines to match this asymmetric structural distribution, we produced a model that predicts extension axes consistent with the vein orientation (Fig. 13c). However, observed vein widths are significantly less than we would expect from the strain ratios shown in this flexural flow model.

5.4. SEM and microprobe

In addition to examining fold shape and fabric distribution, we used a scanning election microscope (SEM) and a JEOL 8900 Electron Microanalyzer (commonly referred to as a microprobe) to make photomicrographs and to measure element spectra at various locations around folds A and C. In particular, we were looking for microfabric information and for evidence of pervasive dissolution/reprecipitation. We wanted to investigate the possibility of diffuse, non-localized chemical redistribution of material (essentially 'homogeneous tangential longitudinal strain') around these folds as a folding mechanism.

Fold A is composed of calcite, quartz, and minor amounts of pyrite and dolomite, with traces of apatite and potassium feldspar or kaolinite (Fig. 14a). Mineral composition is approximately constant along the layering, which we interpret to indicate that no diffuse dissolution has occurred in the fold hinge zone. Calcite/quartz ratios vary as grain size changes normal to bedding, with finer grain sizes corresponding to lower calcite content. These changes (in grain size and calcite content) occur at two primary (stratigraphic) boundaries, rather than gradually over the thickness of the layer (Fig. 14b). Again, this change is consistent with a lack of mineralogical redistribution by tectonically driven chemical processes.

In fold C, the rock consists of a more complex mineralogy, including quartz, calcite, phyllosilicate minerals of various compositions, and minor amounts of rutile, apatite, and pyrite. A rough alignment of angular quartz grains forms a subtle bedding-parallel fabric (Fig. 15a). In the fine-grained layers, which have higher phyllosilicate abundance, this fabric is strongly defined in those mineral phases, but is oblique to bedding (Fig. 15b). Again, mineral composition is approximately constant along bedding, and varies stepwise across bedding at distinct boundaries between finer and coarser grained layers. As in fold A, these features are consistent with a lack of mineralogical redistribution, on the layer scale, by tectonically driven chemical processes.

6. Discussion

6.1. Folding style

All three of the folds that we examined are from the flanks of the Wills Mountain Anticline, and were deformed during the Alleghanian orogeny (c.f. Perry, 1978; Banks and Warburton, 1986; Kulander and Dean, 1986; Mitra, 1986; Geiser, 1988a,b; Dunne, 1989, 1996; Ferrill and Dunne, 1989; Groshong Jr. and Epard, 1992; Wilson and Shumaker, 1992; Smart et al., 1997). Each fold contains some combination of veins, stylolites, and evidence of bed-parallel slip, while lacking evidence for pervasive tectonic fabrics, which we interpret to mean that the same deformation mechanisms were operative in all three folds. Thus, any differences in folding behavior and structural development should be due to lithological (compositional, and consequent rheological) differences, layer thickness, or multilayer versus single layer configuration, rather than temperature, pressure, or strain rates.

The three folds we analyzed are from Silurian carbonate units. Since these folds formed within the same large-scale structure, in similar conditions, and since they have similar accommodation structures, they offer us the opportunity to compare the nearly simultaneous development of three different natural folds. It is especially interesting, therefore,

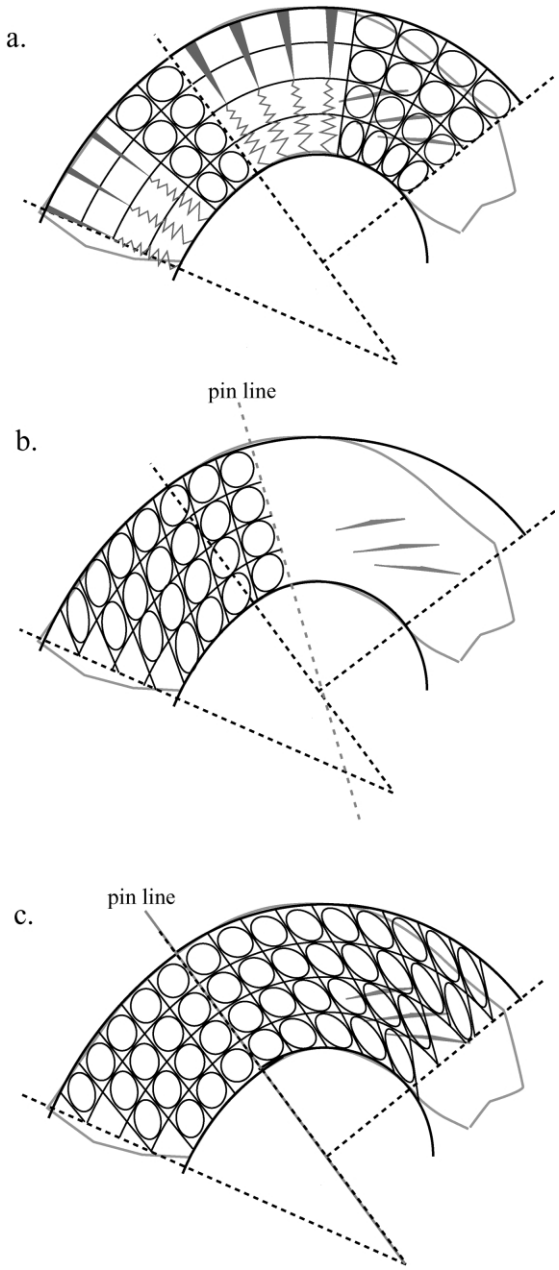

Fig. 13. Fold C, with various fold models superimposed. (a) Tangential longitudinal strain. (b) Flexural flow, pinned at the hinge. (c) Flexural flow, pinned on one limb.

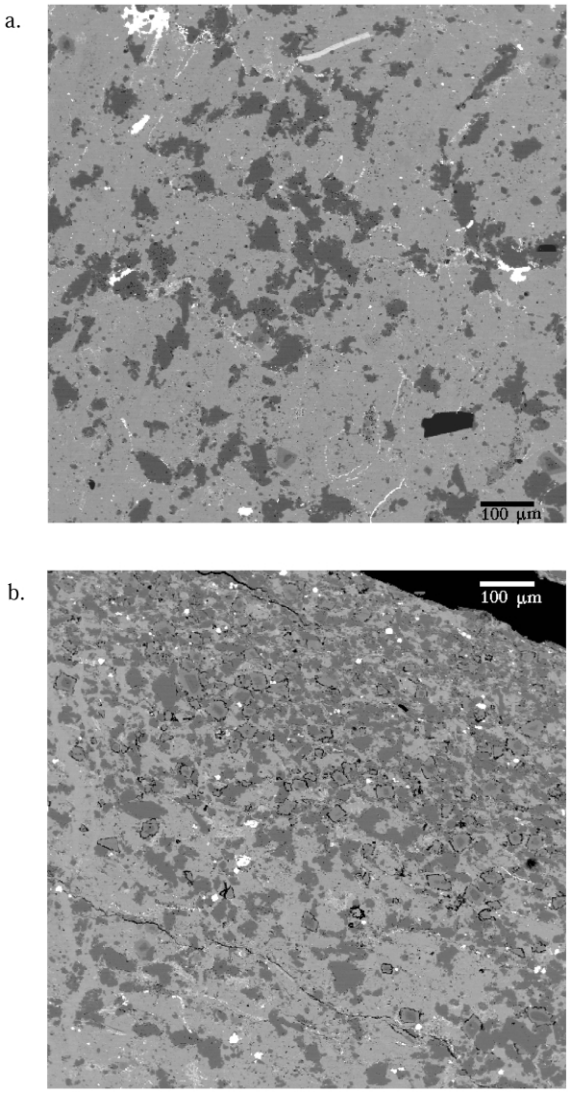

Fig. 14. Microprobe images of fold A. (Locations of probe sites are shown in Fig. 5.) (a) The bulk of the rock is composed of quartz (dark gray) and calcite (medium gray). Minor pyrite (bright spots) and dolomite (zoned rhombs). (b) Mineralogy changes with grain size. Dolomite (zoned crystals with black outlines) are more common in fine-grained beds.

that each fold has a unique geometry and distribution of structures. Fold A is the only one with well-developed bed-normal stylolitic surfaces, and also has the most asymmetric overall shape. Fold B has the most symmetric distribution of veins, consistently normal to bedding, and is the only fold where undulose extinction is common within the veins. Fold C has a regularly spaced set of veins in one limb.

Our interpretation of these three examples is that the single layer folds deformed largely by flexural flow, whereas the individual layers within the multilayer fold under the same temperature, pressure, and strain rate conditions deformed by tangential longitudinal strain. In all cases, stylolite and vein formation were the mechanisms of strain accommodation. Moreover, slip must have occurred between layers in the multilayer fold. In this situation, where tangential longitudinal strain occurs within layers, but flexural slip occurs between layers, the 'dominant' deformation mechanism is a matter of scale of observation (Hudleston et al., 1996). Furthermore, although these folds all occur on the flanks of a large-scale asymmetric fold, this natural asymmetry is more obviously reflected in the shape and strain distributions of the single layer folds than in the multilayer. We do not know whether this is true more generally, or if it is coincidental to these folds.

If an isolated perturbation grows as a small fold on the limb of a much larger fold, it will likely develop asymmetry that reflects the sense of shear associated with strain

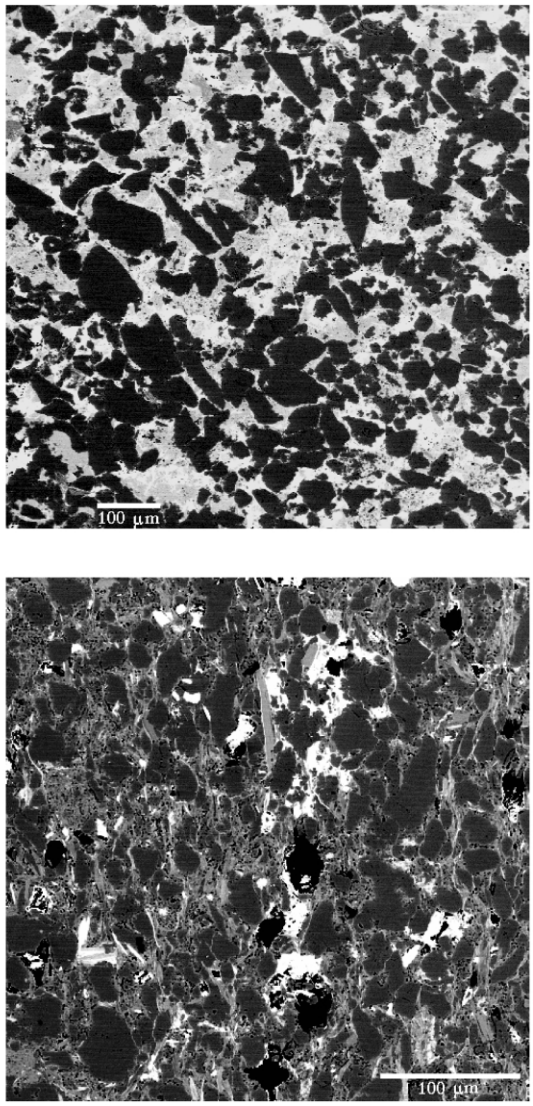

Fig. 15. Microprobe images of fold C. (Locations of probe sites are shown in Fig. 5.) (a) Coarse-grained layers are dominated by quartz (dark gray), with calcite (medium gray) and clay or phyllosilicate matrix (various shades of light to medium gray, depending on chemistry). (b) Fine-grained layers exhibit strong alignment of phyllosilicates.

development in the larger fold. Moreover, this asymmetrical growth is likely to result in a concentration of strain in the short limb of the small fold. This limb represents the greatest deviation of bedding from local 'regional' bedding, which is the attitude of the limb of the larger fold on which the small fold is located. Thus we expect that, if there is asymmetry of strain, it will be greater in the short limb than in the long limb. This is what we see in fold A, and what is likely the case also in fold C.

6.2. Rheology

In this study, we also attempted to obtain rheological information from fold geometry. Previous workers have shown that average arclength to thickness (L/h) ratios, hinge curvature, and relative proportions of limb length to hinge zones (for a given overall shortening) are useful indicators of rheological behavior of a buckled single layer and its matrix (e.g. Ramsay, 1967; Fletcher and Sherwin, 1978; Cruikshank and Johnson, 1993; Hudleston and Lan, 1994; Lan and Hudleston, 1995b). For our two single-layer samples, layer shortening prior to fold amplification was small, and observations in outcrop suggest that the measured L/h of 5.6 for fold A is typical. These two features are consistent with the competent limestone layer behaving in a highly non-linear manner (Hudleston and Holst, 1984). They are inconsistent with Newtonian rheology.

Hinge sharpness is sensitive to non-linearity of the flow law at larger values of L/h—specifically, fold hinges become sharper and limbs straighter as the stress exponent in the flow law for the layer increases—but when $L/h < 10$, fold hinge shape becomes insensitive to rheology (Lan and Hudleston, 1995a). Thus the curvature in the hinge of folds A and C cannot be used to corroborate inferences about non-linearity.

7. Conclusions

We studied three small folds from the flanks of the Wills Mountain Anticline, in the Appalachian Valley and Ridge province. Each of the three folds we examined can geometrically be fit to a variety of fold development models. However, each fold also contains structural clues to its kinematic history. We use both fold shape and distribution of meso- and microstructures to infer fold development. We interpret folds A and C to have developed by asymmetric flexural flow, with local pin lines at some distance from the axial planes. Fold A also appears to have undergone a late hinge-tightening by localized dissolution. We interpret fold B, on the other hand, to have formed by flexural slip between layers, within which deformation was accommodated by outer arc extension, all of which was followed by late-stage heterogeneous flattening.

In fold A, a preponderance of veins in the short limb of the fold, the orientations of these veins, slickenlines on the bedding surface normal to the fold axis, and stylolites that crosscut some of the veins are all consistent with folding by asymmetric flexural flow, later tightened by localized dissolution. The en échelon veins in one limb of fold C, dipping toward the axial surface, are similarly suggestive of asymmetric flexural flow. Development by tangential longitudinal strain would be inconsistent with extension directions in these folds. Microprobe analyses show that mineral content also does not vary as we would expect it to in the case of pervasive inner arc dissolution and outer arc precipitation, thus supporting a flexural flow mechanism as well. In contrast to the structures in these single-layer folds, the wedge-shaped, bed-normal veins in fold B are suggestive of a component of outer arc extension (tangential

longitudinal strain plus volume gain) in that fold's development. For fold B, we also infer a late-stage 'flattening' episode from tabular bed-normal veins in the limbs, bedding-parallel stylolites that crosscut some veins, and undulose extinction of some vein calcite.

We feel it is particularly important to emphasize that different layers may deform quite differently under virtually identical conditions. These differences in deformation may include, but are probably not limited to, which deformation mechanism will be most active. These differences in mechanisms in turn depend on layer configuration (thickness and spacing) and composition. It is uncertain from this study whether, in general, single layer folds are more likely than multilayer folds to deform asymmetrically, and also whether they are more likely to deform by flexural flow. It also may be the case that the 'dominant' deformation mechanism depends, in part, on the scale of observation. For example, the layers in fold B, our multilayer fold, likely underwent flexural slip, whereas internally each of those layers deformed by outer arc extension. It is therefore crucial to consider scale of observation in one's analyses of fold histories.

Acknowledgements

This study was partially supported by grants #EAR9219702 and EAR9526945 from the National Science Foundation. Steve Wojtal and Labao Lan assisted in the collection of these samples. We thank Bill Dunne, Nick Woodward, and two anonymous reviewers for their constructive comments on early versions of this manuscript.

References

Banks, C.J., Warburton, J., 1986. 'Passive-roof' duplex geometry in the frontal structures of the Kirthar and Sulaiman mountain belts, Pakistan. Journal of Structural Geology 8, 229–237.

Cruikshank, K.M., Johnson, A.M., 1993. Simulation of high-amplitude folding in viscous multilayers. Journal of Structural Geology 15, 79–94.

Dewey, J.F., 1965. Nature and origin of kink-bands. Tectonophysics 1, 459–494.

Dietrich, D., 1986. Calcite fabrics around folds as indicators of deformation history. Journal of Structural Geology 8, 655–668.

Dunne, W.M., 1989. Valley and Ridge Province in eastern West Virginia. In: Engelder, T. (Ed.), Structures of the Appalachian Foreland Fold-Thrust Belt, Field Trip Guidebook T166, 28th International Geological Congress, pp. 53–61.

Dunne, W.M., 1996. The role of macroscale thrusts in the deformation of the Alleghanian roof sequence in the central Appalachians: a re-evaluation. American Journal of Science 296, 549–575.

Dunne, W.M., Ferrill, D.A., 1988. Blind thrust systems. Geology 16, 33–36.

Engelder, T., 1989. Foreword: structures of the Appalachian Foreland Fold-Thrust Belt. In: Engelder, T. (Ed.), Structures of the Appalachian Foreland Fold-Thrust Belt, Field Trip Guidebook T166, 28th International Geological Congress, pp. 1–2.

Ferrill, D.A., Dunne, W.M., 1989. Cover deformation above a blind duplex: an example from West Virginia, USA. Journal of Structural Geology 11, 421–431.

Fisher, D.M., Anastasio, D.J., 1994. Kinematic analysis of a large-scale leading edge fold, Lost River Range, Idaho. Journal of Structural Geology 16, 337–354.

Fletcher, R.C., Sherwin, J., 1978. Arc length of single layer folds: a discussion of the comparison between theory and observation. American Journal of Science 278, 1085–1098.

Geiser, P.A., 1988. The role of kinematics in the construction and analysis of geological cross-sections in deformed terranes. In: Mitra, G., Wojtal, S. (Eds.), Geometries and Mechanisms of Thrusting, With Special Reference to the Appalachians. Geological Society of America Special Paper 222, pp. 47–76.

Geiser, P.A., 1988b. Mechanism of thrust propagation: some examples and implications for the analysis of overthrust terranes. Journal of Structural Geology 10, 829–845.

Geiser, J., Geiser, P.A., Kligfield, R., Ratliff, R., Rowan, M., 1988. New applications of computer-based section construction: strain analysis, local balancing, and subsurface fault prediction. Mountain Geology 25, 47–59.

Gray, D.R., 1981. Cleavage-fold relationships and their implications for transected folds: an example from southwest Virginia, USA. Journal of Structural Geology 3, 265–277.

Groshong Jr, R.H., 1975. Strain, fractures, and pressure solution in natural single-layer folds. Geological Society of America Bulletin 86, 1363–1376.

Groshong Jr, R.H., Epard, J.-L., 1992. Implications of area balance for strain and evolution of detachment folds. Geological Society of America, Abstracts with Programs 24, A246.

Hudleston, P.J., Holst, T.B., 1984. Strain analysis in buckle folds and implications for the rheology of the layers during folding. Tectonophysics 106, 321–347.

Hudleston, P.J., Lan, L., 1993. Information from fold shapes. Journal of Structural Geology 15, 253–264.

Hudleston, P.J., Lan, L., 1994. Rheological controls on the shapes of single-layer folds. Journal of Structural Geology 16, 1007–1021.

Hudleston, P.J., Tabor, J.R., 1988. Strain and fabric development in a buckled calcite vein and rheological implications. Bulletin of the Geological Institute, University of Uppsala, N.S. 14, 79–94.

Hudleston, P.J., Treagus, S.H., Lan, L., 1996. Flexural flow folding: does it occur in nature? Geology 24, 203–206.

Kulander, B.R., Dean, S.L., 1986. Structure and tectonics of central and southern Appalachian Valley and Ridge and Plateau Provinces, West Virginia and Virginia. Bulletin of the American Association of Petroleum Geologists 70, 1674–1684.

Lan, L., Hudleston, P.J., 1995a. A method of estimating the stress exponent in the flow law for rocks using fold shape. Pageoph 145, 621–635.

Lan, L., Hudleston, P.J., 1995b. The effects of rheology on the strain distribution in single layer buckle folds. Journal of Structural Geology 17, 727–738.

Markley, M., Wojtal, S., 1996. Mesoscopic structure, strain, and volume loss in folded cover strata, Valley and Ridge Province, Maryland. American Journal of Science 296, 23–57.

McConnell, D.A., Kattenhorn, S.A., Benner, L.M., 1997. Distribution of fault slip in outcrop-scale fault-related folds, Appalachian Mountains. Journal of Structural Geology 19, 257–267.

Mitra, S., 1986. Duplex structures and imbricate thrust systems: geometry, structural position, and hydrocarbon potential. Bulletin of the American Association of Petroleum Geologists 70, 1087–1111.

Narahara, D.K., Wiltschko, D.V., 1986. Deformation in the hinge region of a chevron fold, Valley and Ridge Province, central Pennsylvania. Journal of Structural Geology 8, 157–168.

Oertel, G., 1974. Unfolding of an antiform by the reversal of observed strains. Geological Society of America Bulletin 85, 445–450.

Onasch, C.M., 1984. Petrofabric test of viscous folding theory. Tectonophysics 106, 141–153.

Perry, W.J., Jr., 1978. The Wills Mountain Anticline: a study in complex folding and faulting in eastern West Virginia. West Virginia Geological and Economic Survey Publication RI-3.

Ramsay, J.G., 1967. Folding and Fracturing of Rocks, McGraw-Hill, New York.

Sanderson, D.J., 1982. Models of strain variation in nappes and thrust sheets: a review. Tectonophysics 88, 201–233.

Scott, P.B., Dunne, W.M., 1990. Deformation history of an outcrop-scale fault system in the Central Appalachians. Southeastern Geology 31, 93–107.

Simon, R.I., Gray, D.R., 1982. Interrelations of mesoscopic structures and strain across a small regional fold, Virginia Appalachians. Journal of Structural Geology 4, 271–289.

Smallshire, R.J., 1997. Rolling hinges as a mechanism for buckle growth: evidence from the Haut Giffre, French Alps. 29th Annual Meeting of the Tectonics Studies Group of the Geological Society of London.

Smart, K.J., Dunne, W.M., Krieg, R.D., 1997. Roof sequence response to emplacement of the Wills Mountain duplex: the roles of forethrusting and scales of deformation. Journal of Structural Geology 19, 1443–1459.

Suppe, J.S., 1983. Geometry and kinematics of fault-bend folding. American Journal of Science 283, 684–721.

Thorbjornsen, K.L., Dunne, W.M., 1997. Origin of a thrust-related fold: geometric vs. kinematic tests. Journal of Structural Geology 19, 303–319.

Williams, P.F., 1979. The development of asymmetrical folds in a cross-laminated siltstone. Journal of Structural Geology 1, 19–30.

Wilson, T.H., Shumaker, R.C., 1992. Broad top thrust sheet: an extensive blind thrust in the Central Appalachians. American Association of Petroleum Geologists Bulletin 76, 1310–1324.

Yin, A., Oertel, G., 1993. Kinematics and strain distribution of a thrust-related fold system in the Lewis thrust plate, northwestern Montana (USA). Journal of Structural Geology 15, 707–719.